FLORIDA STATE UNIVERSITY

COLLEGE OF ENGINEERING

DESIGN AND CHARACTERIZATION OF A VARIABLE STIFFNESS APPLICATION FOR A DYNAMIC RUNNING ROBOT

By

JASON NEWTON

A Honor's Thesis submitted to the
Department of Mechanical Engineering
in partial fulfillment of the
requirements for graduation with
Honors in the Major

Degree Awarded:
Spring Semester, 2012

ABSTRACT

Research has shown that being able to vary the effective limb stiffness of legged robotics can aid in efficient locomotion. This is especially true when considering a variety of terrains and payloads. Recent developments have lead to multiple solutions for implementing variable compliance mechanisms, including mechanically actuated methods as well as smart materials. These methods have typically been directed toward moderately large, dynamic running platforms. Less work has been performed on small scale robotics.

This work presents the design of a a new robotic leg mechanism for a variable stiffness application. The design utilizes dielectric elastomer (3M VHB 4910) pre-stretched into a diaphragm to rapidly control stiffness changes for enhanced mobility and agility of a field demonstrated, small scale hexapod robot, iSprawl. The diaphragms developed are modular in nature to allow for fine tuning of the permissible stiffness range. A set of electro-mechanical test are utilized to obtain up to 92% reduction in stiffness that is controlled by an electric field. Preliminary transient tests are used to characterize the response time of the system when exposed to sudden field application. The device achieves a full transition to a decreased stiffness approximately $66ms$ post field application. This work demonstrates a functional mechanism for exhibiting tunable compliance on a reduced scale architecture and outlines the necessary methods for future implementation.

Keywords: Robot, Stiffness, Dielectric elastomer

The members of the committee approve the dissertation of Jason Newton defended on April 13, 2012.

Dr. Jonathan Clark
Professor Directing Honor's Thesis

Dr. William Oates
Committee Member

Dr. Mei Zhang
Committee Member

TABLE OF CONTENTS

LIST OF TABLES

LIST OF FIGURES

CHAPTER 1

INTRODUCTION

1.1 Goals

This work is devoted to developing a platform inspired mechanism for integrating variable compliance into the limbs of a small scale robot. To keep pace with the rapid evolution of robotic platforms, the mechanism will implement a next generation actuator using smart materials. The addition of smart materials would aid in the advancement of robots built for multi-terrain applications while providing a lightweight, robust versatility not currently found in systems with fixed compliance. This research proposes a design for implementation on a small scale dynamic running robot and further characterizes its capabilities as a variable stiffness mechanism.

1.2 Background

1.2.1 Variable Stiffness

Robotics tend to look toward biology as a model for performance. Animals frequently demonstrate a level of adaptability that is unmatched by current robotic designs. While a system may be constructed for a certain task on a certain terrain, slight deviation from those preset parameters can result in a drastic decrease in performance. When looking into the mechanisms utilized by animals running over various terrains, passive stiffness rises as a modifiable factor. Animals have been shown to rely on properly tuned leg springs in order to achieve effective running [1, 2]. Furthermore, studies show that humans adapt their overall leg stiffness when confronted with surfaces of varying compliance [3]. Similar research on humans has been performed focusing on the the natural adaption of leg compliance when landing on differing surfaces, demonstrating that rapid adjustment occurs in an attempt to

aid in the dissipation of energy [4]. In order for robotic system to emulate these types of adaptations of their passive leg compliance, a variable stiffness mechanism is required. A wide range of possibilities exist for implementing such a mechanism. One possible solution is the inclusion of mechanical actuation to change the passive limb parameters.

1.2.2 Mechanical Solutions

Multiple approaches have been taken for fabrication of a mechanically varied mechanism including the combination of motor driven pulleys and springs [5] and a system implementing geometric constraints to control limb compliance [6]. The robotic platform Edubot,depicted in Figure 1.1, implemented a novel mechanical design for varying the passive leg compliance [6]. This platform is of particular interest due to both the experimental and simulation data available on variable stiffness. The mechanism, seen in Figure 1.2 uses a worm gear and motor attached to each leg as the actuator. Rotation of the worm gear adjusts the location of a slider which acts to adjust the approximate bending location along the C-leg.

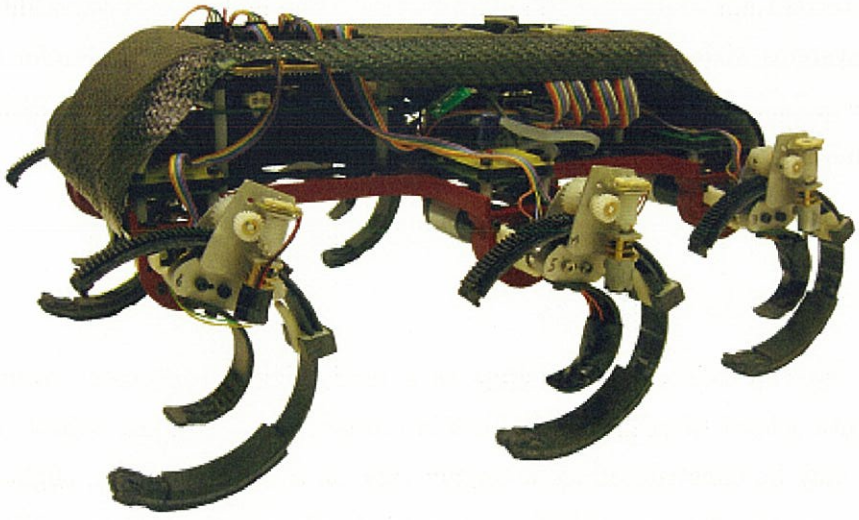

Figure 1.1: Hexapedal robotic platform, EduBot. The legs utilize a mechanically actuated variable stiffness mechanism. The worm gears located in each leg adjust the position of a slider which controls the effective bending location on each C-leg, changing the relative limb compliance. [7]

Tests were performed on the platform to develop a knowledge of the ideal stiffness for various terrains and weight constraints [7]. All experiments were performed with respect

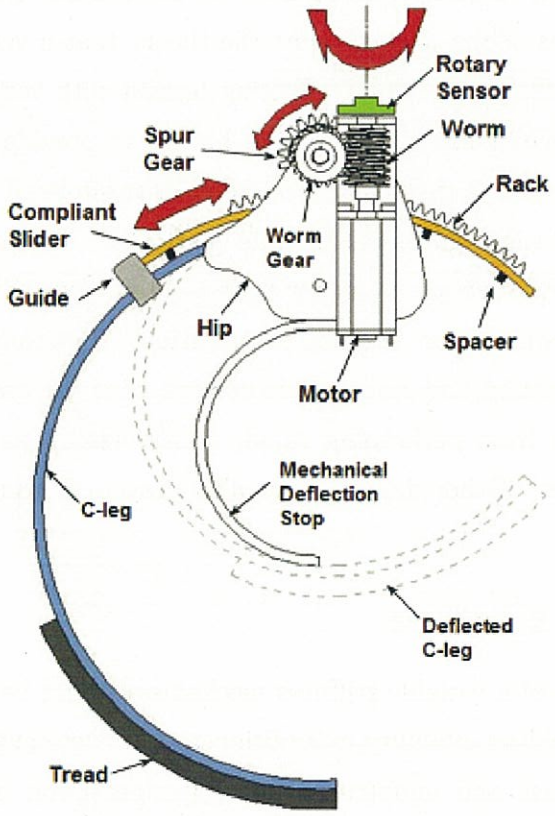

Figure 1.2: Diagram depicting variable stiffness leg mechanism implemented onto the edubot platform. The slider-guide combination allow for the effective stiffness variation. A mechanical stop is in place to prevent over compression of the C-leg when in its most compliant state. [7]

to a single relative stiffness, which corresponded to approximately $1280\frac{N}{m}$. Using this method an achievable stiffness range of $640\frac{N}{m}$ to $1113.6\frac{N}{m}$ was found to be desirable. This ranges were determined through a fractional multiplier to the relative stiffness. The values correspond to 0.5 and 0.87 multiplier for the lower and upper bounds, respectively. This work demonstrated that by decreasing the effective leg stiffness can yield similar efficiencies when traveling at varying speeds. For the purpose of this work the efficiency was quantified using specific resistance. The tests were performed on carpet, padding, and grass surfaces, while attempting to optimize forward velocity. Another parameter varied within this work was the presence of a $0.91kg$ payload. A variation in stiffness when carrying the payload caused

a specific resistant drop to below that seen in the unburdened system on the same terrain. The overall conclusions of the work support the theory that a variation of leg stiffness can be used to optimize efficiencies when traversing terrain with varying compliance with and without a payload. While this unique design helped to provide studies into the required stiffness ranges for a dynamic running robot, the mechanism itself has drawbacks that would prevent its implementation onto smaller scale platforms. The required single motor and gear box per leg would overburden smaller hexapedal robots. Other restrictions arise with the actuation time required for compliance variation. Typically the platform pauses to perform the reconfiguration and resumes locomotion once the procedure is complete. This would inhibit a robot from performing rapid, in-situ variations to accommodate sudden environmental changes. Other designs have also proven themselves relatively bulky and fragile [5].

1.2.3 Material Solutions

More preferable traits of a variable stiffness mechanism would be demonstrated in a design that could exhibit rapid adaptability in addition to a robust construction. The mechanism should also be compact and unobtrusive for implementation onto the limbs of smaller platforms. The mechanism should also be lightweight, as to not hinder locomotion or detract from the overall potential payload. Because of these requirements, a smart material solution presents itself as a viable option for a variable compliance structure.

Shape Memory Polymer

Shape Memory Polymers (SMPs) show great potential for variable stiffness structures due to their inherrent physical properties. In general they demonstrate the capability to undergo large amounts of deformation while remembering the original pres-set shape. The process experienced by a deformed SMP composite can be seen in Figure 1.3. These materials can be designed to respond to a range of stimuli including magnetic, electrical, water/solvent, thermal, and light [8, 9]. The most common of these tend to be the thermally actuated SMPs. The mechanism is first designed by presetting the "original shape". In the case of fiber composites, this involves the development of the SMP in a resin-like form and infusion into a fiber weave. Once the initial shape is set, the system can be heated past its transition temperature which causes the cross-linking agent to enter an amorphous liquid phase. This

provides the means to achieve great flexibility with limited resistance. Upon cooling in a deformed state (referred to as storage in Figure 1.3), internal stresses arise due to the reconfiguration of the cross linking agent. When heated past the transition temperature once more, the stresses promote a self realignment of the material to its original shape (referred to as recovery in Figure 1.3).

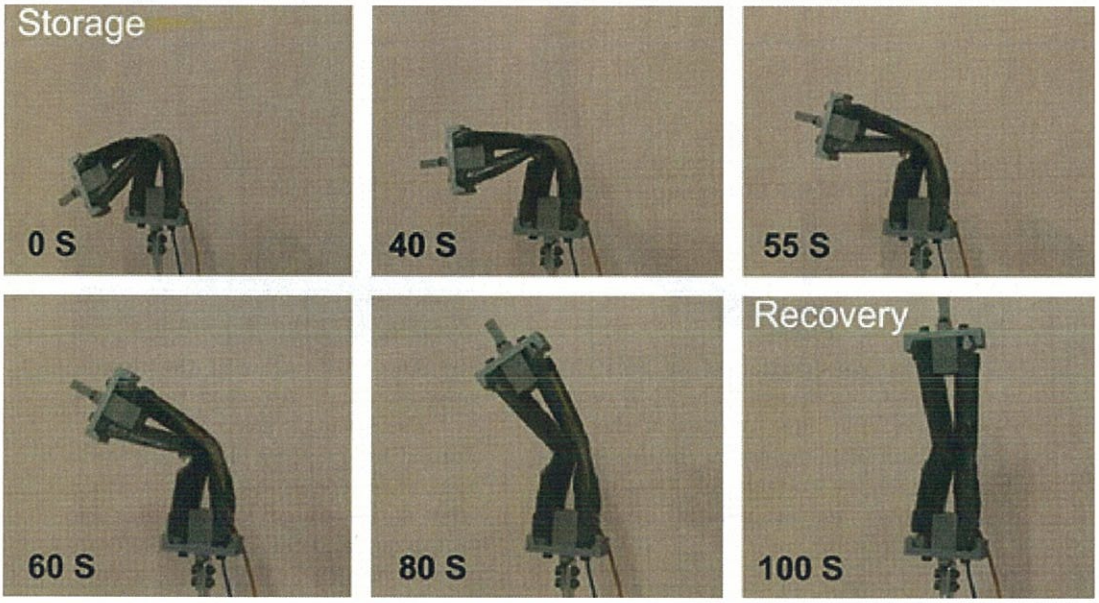

Figure 1.3: A depiction of the SMP recovery process. The process moves from left to right, top to bottom. The upper left picture represents the the deformed state with stored internal stresses. As heating occurs the cross-linking agent liquefies and allows the reconfiguration of the material to is original, zero stress state. [8]

Recent developments have utilized SMP as an alternative solution to a variable stiffness C-leg design [10]. In this work a section of SMP composite was integrated into C-leg architecture at a primary flexure point. The composite leg design is depicted in Figure 1.4a. The design was constructed with a length of heating element molded onto the surface of the SMP section along with a thermocouple. Controlled by a Pololu Baby-Orangutan microprocessor, the SMP segment was heated to increase compliance. A depiction of the leg with the necessary wiring can be seen in Figure 1.4b. The achievable stiffness range included the maximum value of $2310\frac{N}{m}$, which corresponded to no heating, and a minimum stiffness of approximately $600\frac{N}{m}$.

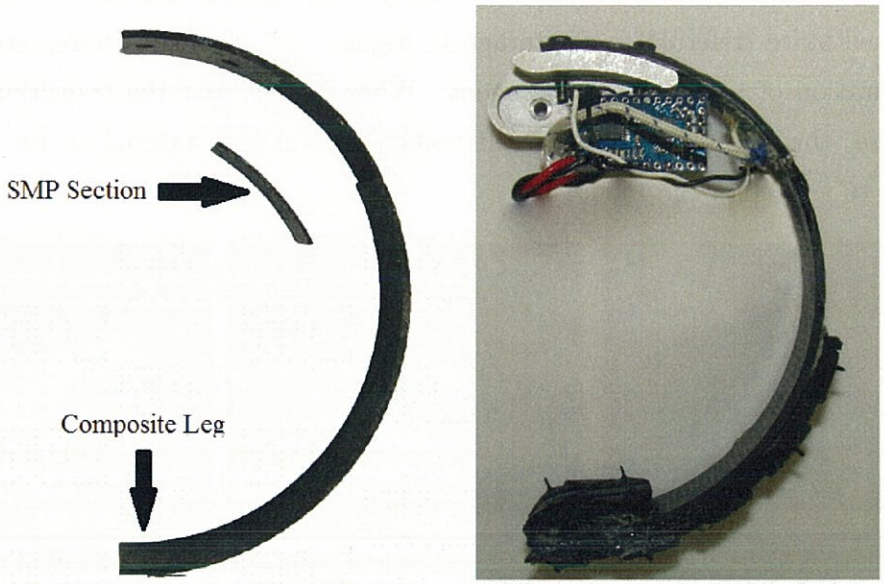

(a) The construction of an SMP integrated C-leg design. The SMP section fits into the inner portion of the c-leg to maintain compression on the segment throughout a loading cycle. This helps to prevent delamination during cyclic loading.

(b) The SMP leg with the associated circuitry. Attached to the leg is a thermocouple for measuring the current temperature of the SMP section, wires connected to the heating element integrated into the surface of the leg, and the Baby Orangutan microcontroller for heating control.

Figure 1.4: The multiple stages of construction for the SMP C-Leg design. [10]

Since the actuation methods simply involved a current supply, the transition could be performed in motion as compared to the mechanical design. Furthermore, the necessary components for each leg are a heating element and thermocouple, while a centrally mounted microcontroller could govern all the legs, the amount of weight added to the system could be relatively negligible. The downfalls of this system arise during activation. The actuation time required for the system demonstrated a certain degree of hysteresis due to the thermodynamic properties of the material. Heating, and therefore an increase in compliance, could be performed relatively quickly, but the increase in stiffness was directly dependent upon the temperature of the SMP section. This yielded a system that was effectively hindered by its capacity for heat dissipation. Mechanical problems were also experienced during experimental testing of the composite legs. The high impact load associated with the bipedal

runner used for testing resulted in small amounts of delamination at the SMP-leg interface. However, the design was susceptible to fatigue loading and needed further improvement to increase durability. For systems operating with a higher frequency, it would be more favorable to remove the time required for cooling.

Dielectric Elastomers

Dielectric Elastomers represent a collection of materials which could offer both lightweight mechanisms as well as decreased actuation times. There are multiple types of dielectric elastomers available for use, the most commonly used are Dow Corning HS3 silicone, Nusil CF 19-2186 silicone, and 3M VHB 4910 acrylic [11]. For the purpose of this work, VHB 4910 was the primary candidate due to its high breakdown strength, availability, and its relatively low cost. The dielectric elastomers utilize an electric stimuli to promote a physical response. If a flexible electrode is spread over the surface of the elastomer, a geometric reconfiguration occurs when an electric field is applied. This is demonstrated visually in Figure 1.5. The high potential fields create an attractive force between the two electrodes. When this force is coupled with both the natural compliance of the system and a tendency to retain a constant volume, the electrostatic forces compress the membrane in a direction parallel to the applied voltage field. This compression results in an overall expansion in the planar directions. If the boundaries of the membrane are constrained to a predetermined size, as the specimen displaces it produces an effective stiffness change. The magnitude of the voltage required to induce a significant compression is typically greater than $1kV$ [12]. VHB is capable of 100% or greater deformation under a field on the order of 10-100MV/m. However, if the field is too great, it motivates dielectric breakdown of the membrane. The maximum allowable field is on the order of $350\frac{MV}{m}$ for silicone and $440\frac{MV}{m}$ for VHB[11]. The induced expansion can be altered by implementing a prestrain into the system, typically perpendicular to the electric field. The addition of a unidirectional prestrain can constrain the majority of the expansion in the unstrained axis, allowing for a greater level of control [13]. The presence of prestrain can both aid and hinder the membrane configuration. With increasing prestrain, the required field to manifest a reaction decreases, however it also shares a inverse relationship with the dielectric breakdown regime. Further incrementation of the prestrain reduces the maximum allowable field application. The actuation speed of VHB presents itself as a reasonable candidate for relatively rapid applications, being on the order of 10's of Hz. The VHB

membrane is reliable under stresses up to 1 MPa [11], but it is best suited for lightweight applications as the uncompressed thickness tends toward the scale of millimeters or less.

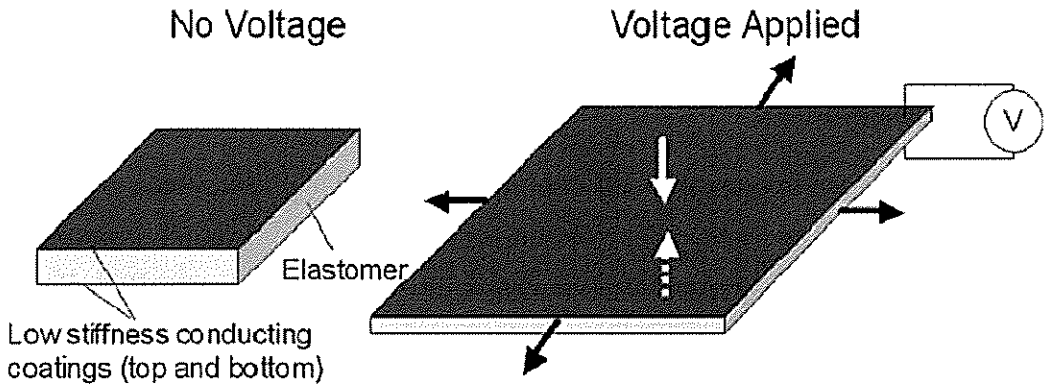

Figure 1.5: A depiction of VHB before prior (left) and post(right) field application. The surface is coated with a flexible electrode and once a electric field is present, an out of plane compression occurs. This compression induces an planar expansion of the material. [11]

VHB is capable of being implemented in numerous configurations, allowing for a wide variety of potential applications. Some examples of these are the "Spring Roll" design from Figure 1.6, wherein a section of VHB is wrapped around the circumference of a helical spring [13]. Depending on how the system is actuated, bending occurs in a prescribed direction. Similar designs have also been created to act as a linear actuator for legged robotics, while more planar configurations have yielded designs intended as serpentine manipulators and flapping wing mechanisms [14]. A configuration that is more applicable to the present work is a suspended membrane contained within a diaphragm. Further discussion on this design and its capabilities is provided in Chapter 2.

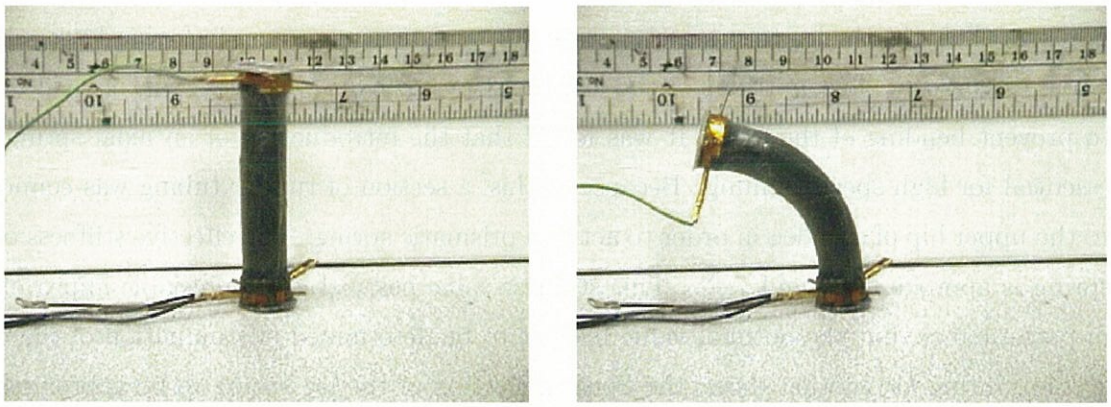

Figure 1.6: The Spring Roll configuration of the dielectric elastomer, VHB 4910. The membrane encompasses the outer surface of a helical spring and when activated, results in a controllable bending motion. The left figure shows the unactuated mechanism where the right figure captures the deformed state. [13]

1.2.4 iSprawl Platform

Little work has been performed on adapting the iSprawl platform for variable compliance. iSprawl, depicted in Figure 1.7, is a biomimetic hexapedal running robot which, like RHex, is modeled using the dynamics found in cockroaches [15]. Since the iSprawl platform shares similar characteristics with both RHex and EduBot, the previous research could be used as a starting point for incorporating a variable stiffness mechanism with this robot. Even though iSprawl may share inspiration with the previous hexapedal platforms, the physical parameters are drastically different. It has an approximate mass of 0.3 kg and a top speed of 2.3 m/s (15 body lengths/sec). The locomotion methods rely on the six leg wires being thrust downward in an alternating tripod gate. The driving mechanism consisting of a double crank assembly attached with a 180^o phase shift. The leg wires are flexible in nature, extending from the drive system through individual sections of low friction tubing which help to reorient the driving motion in the necessary direction. A visual representation of the driving mechanism and routing path for the leg wires can be seen in Figures 1.7a and 1.7b. The wires are attached through the center of shape deposition manufactured (SDM) legs to provide a rigid mounting surface, thereby constraining the direction of the locomotive forces. The SDM legs incorporate sections of both rigid and compliant geometries. The compliant

portions allow the the leg to passively rotate during extension, aiding in forward propulsion. Upon exiting the inner portions of the leg, the wire is affixed with a section of rigid casing to prevent bending of the limb. It was found that the introduction of an axial spring was essential for high speed running. Because of this, a section of rubber tubing was connected to the upper hip of each leg in order to act as a prismatic spring. The effective stiffness of the spring is approximated at $1.7\frac{N}{mm}$. This stiffness value has yielded appreciable improvement in performance, but the optimal value has yet to be determined. Examination of the drive system during locomotion shows the linear deflection of the leg spring to be approximately 4 mm.

In the following sections the design, manufacturing methods, and characterization for the dielectric elastomer based variable stiffness robotic mechanism is presented. Section 2 describes the physical architecture of the mechanism and its assembly. Section 3 establishes the experimental setup for the quasi-static electro-mechanical as well as transient tests. Section 4 concludes the results found in this work and establishes the futures goals of the project.

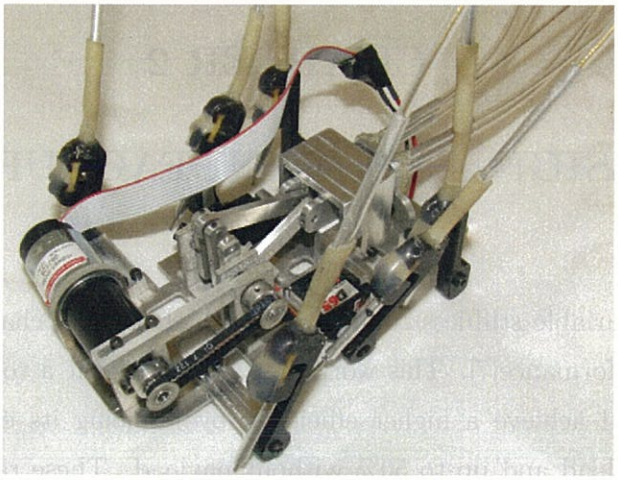

(a) The drive system for iSprawl. It uses a slider crank mechanism with a 180^o phase offset between the two tripods.

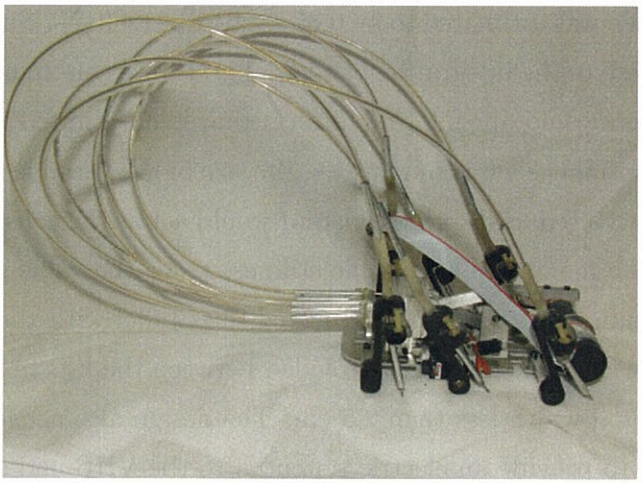

(b) The wire routing path for iSprawl. The low friction tubing can be seen as it guides the wires from the drive system in large loops and toward the legs of the robot.

Figure 1.7: A depiction of the iSprawl platform and its drive system and wiring paths.

CHAPTER 2

DESIGN AND MANUFACTURING

Previous work on variable stiffness running suggests that small changes in stiffness have a large impact on performance[7]. This work demonstrated that a robotic platform utilizing compliant legs could achieve a higher efficiency by reducing its effective leg stiffness by 13% if it had a payload and up to 50% without payload. These ranges also encompassed the desired stiffness modifications for varying types of terrain. Using these ratios, and previous experiments[15], the relative stiffness for iSprawl was set at 1.7 N/mm and the desired stiffness range was estimated to be $0.85\frac{N}{mm}$ to $1.921280\frac{N}{mm}$. Since the desired stiffness should never approach 0, the integration of a variable stiffness mechanism in parallel with the current tubing design would allow for a platform that is not limited to a single ideal terrain for satisfactory performance while minimizing the size of the variable stiffness mechanism. A section of tubing with a reduced spring constant would act as the constraint for the minimum stiffness, allowing the maximum achievable stiffness to be the value gained from the tubing in addition to the number of modules connected in parallel with the tube. Each structure was required to fit within the clearance provided between the legs of iSprawl, restricting the module to have a total width less than 2.5 cm. The design also needed to permit the use of electrodes in a way to provide an electric potential to the VHB and still allow a simple and reliable electrical attachment point. In order to allow for out-of-plane deflection, maximum area for larger deflections, and to allow elastic recovery forces to act equally in all directions, the device was developed using a suspended ring methodology. The overall architecture of a single module is illustrated in Figure 2.1, and a depiction of the methods for assembly is portrayed in Figure 2.3.

2.0.5 Early Iterations

The early designs of the system consisted primarily of ABS plastic cut in a circular orientation. Initially, two symmetric sections would compress the layer of VHB from either side using the natural adhesive tendencies of the membrane. Multiple attempts lead to the realization that the bond formed between the VHB and ABS was not robust enough to maintain any desired prestrain without experiencing slipping. To combat this problem, the frames were redesigning to incorporate four mounting holes for 1.5 *mm* machine screws as seen in Figure 2.2.. This addition permitted the prestrain to be maintained and but presented the danger of conduction points during voltage application. Precautions were taken to prevent conduction through the use of liquid insulation coated around the bolt surface. Even with the addition of insulation methods, the design was deemed undesirable and risky for any type of platform implementation. A second design was required that did not involve puncturing the VHB with a conductive bolt.

The second iteration was designed with a similar geometry, except it was fabricated out of thin aluminum in hopes of providing a better bond with the VHB. This assembly demonstrated the capability to maintain a prestrain without requiring any clamping mechanism.

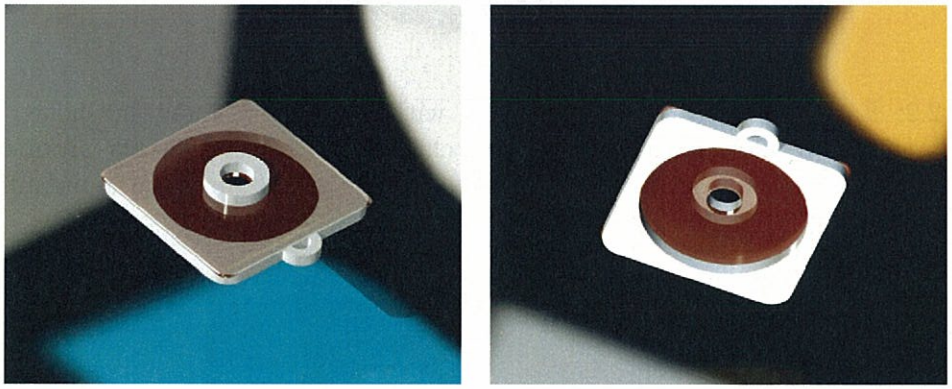

(a) (b)

Figure 2.1: VHB 4910 prestretched and mounted to an aluminum frame. The inner ring acts as the mounting point for the leg wire of iSprawl while the outer frame will be held stationary. The semi-circular tab on the side acts as an external attachment point for the electrical connections. Not pictured here is the insulating Kapton film between the membrane and the frame. Pictures (a) and (b) shows an upper and lower view, respectively.

The problems for this design occurred during field application testing. When connecting the lead wires to the design, the original methods involved a direct placement of the stranded wire to the membrane surface. This caused multiple problems during testing, including undesired detachment of the wire from the membrane and more commonly marring of the VHB surface. The micro-lacerations in the material from the wires added stress concentrations during field application and resulted in frequent electrical arcing and membrane destruction. To limit the burning of samples, a modification needed to be made to accommodate the wire leads. The final design is described in detail in section 2.1

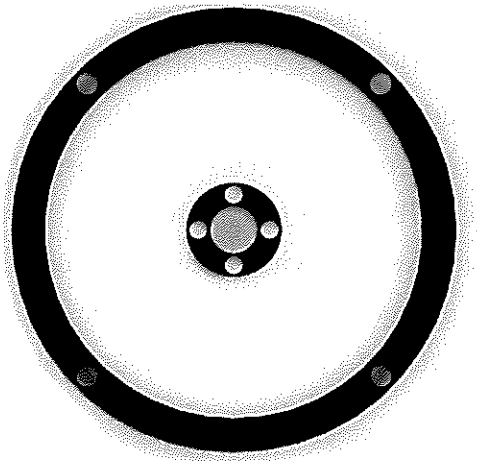

Figure 2.2: Early iteration of module design with inclusion of mounting holes. The holes were fabricated to allow machine screws to clamp two frames together around the VHB membrane. This design held the potential for electrical arcing through the mounting screws.

2.1 Diaphragm Design

The structure was designed to allow for modular implementation; permitting a range of stiffness characteristics to be achieved. Due to the potential application for the iSprawl platform, all designs were based around the constraints mentioned previously. The outer frame was a square with 2.286 cm lengths on all sides. A circular section with a diameter of 1.905 cm was removed from the center for membrane deflection. The small inner ring,

approximately 0.762 cm in diameter, was designed to be attached to the VHB membrane allowing a contact point for manual deflection, while maintaining the biaxial pre-stretch of the membrane. The center of the inner ring was drilled through to allow mounting of the iSprawl leg. Both the inner and outer rings of the system were fabricated from 0.15875 cm ($\frac{1}{16}''$) thick aluminum and polished to prevent abrasive features. With these design parameters, a single modular frame, including both inner and outer rings, added only 1 g to the mass. In order to allow for propagation of the applied field, compliant carbon grease electrodes were painted to the entire exposed area of the VHB using a soft bristled brush to minimize surface damage to the VHB. When coated with the carbon grease electrode, the design allowed for a total active area of 9.576 cm^2. The electrodes were extended to the aluminum frames so that wire leads could be applied to the frame as opposed to directly contacting the VHB. The outer frame was built with a semi-circular hoop onto the outer rim to allow for wire connections. To prevent electric arcing during field application, layers of insulating Kapton film were placed between the VHB membrane and the aluminum frame. The diaphragm mechanism described here is essentially the same design developed by Dastoor and Cutkosky [16]. Implementation of their methods could further decrease the weight and increase the durability for high frequency variable stiffness applications such as the legs for the iSprawl platform.

When stacking modules, the inner rings can be connected together via the leg shaft of the robotic platform. The outer rings could be attached to the input and output leads of an amplifier in an alternating fashion. This is graphically depicted in Figure 2.4a. This methodology would result in the modules behaving similar to springs in parallel, thereby allowing the overall stiffness on the system to be determined by a simple summation of effective spring constants. Series implementation could be achieved by connecting the inner frame to the outer frame of an adjacent module as seen in Figure 2.4. This configuration allows the permissible deflection distance per module to be doubled at the expense of stiffness. Standard spring equations for series implementation would apply for calculating the resulting stiffness.

The assembly as it would be integrated onto the isprawl leg design can be seen in Figures 4.1a and 4.1b. This configuration depicts two modules connected in parallel around the primary leg wire of iSprawl. The presents the concept of having both the variable stiffness mechanism and a tube of constant stiffness connected in parallel to reduce the necessary number of modules. The modules used are an early prototype utilizing the ABS design.

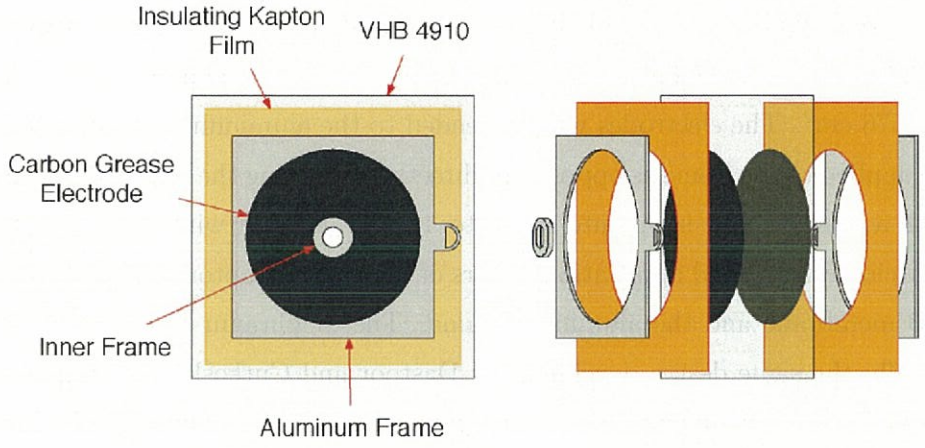

Figure 2.3: Assembly of variable stiffness modular structure. The two aluminum frames are first placed onto kapton thin film as a preventative measure for arcing. The frames are then aligned onto a prestretched membrane of VHB. The inner frame is placed onto a section of unstrained VHB cut to a matching diameter. This is used to provide a soft interface between the sharp edge of the frame and the stretched membrane. Finally, the exposed VHB is painted with carbon grease electrodes on both sides paying special attention to connect the electrode to the inner surface of the frames. The wire leads can then be placed onto the upper and lower frames for voltage application.

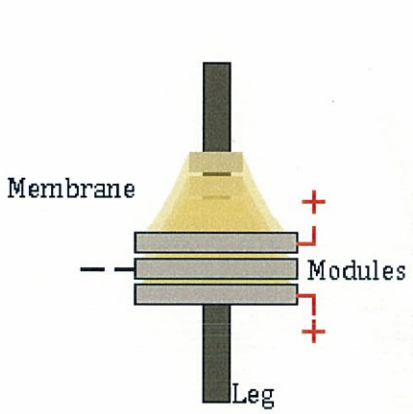

(a) Schematic of modular structures on iSprawl's leg wire attached in parallel

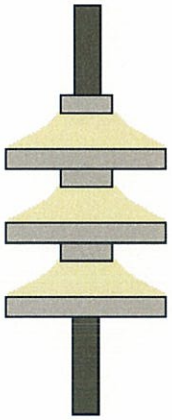

(b) Schematic of modular structures on iSprawl's leg wire attached in series

Figure 2.4: A depiction of the two ways of implementing the variable stiffness modules. Figure (a) represents the parallel formation. The inner rings and outer frames are attached to similar components on adjacent modules. This set up allows for the summation of individual membrane stiffnesses to achieve a more rigid structure. The downfall of this orientation is the reduction in achievable displacement. The maximum displacement is still limited by the possible deflection of a single membrane. Figure (b) shows the series configuration for the modules. The inner frame of a membrane is rigidly attached to the outer frame of the adjacent mechanism. This system presents itself as the most compliant assembly. With increasing number of modules per assembly the overall stiffness will continue to decrease, but the maximum displacement will will sum linearly.

Figure 2.5: Implementation of an early ABS diaphragm design onto an iSprawl leg. Only two modules are shown connected to the leg. The outer frames are connected together via a section of rigid wire. This design was never tested during running, It was only implemented for feasibility purposes.

CHAPTER 3

CHARACTERIZATION

3.1 Experimental Setup

In order to identify the capabilities of the modules the constitutive behavior of the VHB material was characterized. All testing took place using an MTS Insight 1 kN load frame and a 5 N load cell illustrated in Figure 3.1b. The act of loading the sample out of plane is further referred to as transverse loading. Experiments were performed at varying prestrains to determine its effect on both the stiffness and transient properties. The samples examined incorporated three distinct prestretches, 200%, 300%, and 400%. All of which were done in a manner to promote biaxial strains, with uniform stresses throughout the membrane. The experimental testing for this work was performed by Jason Newton and Jeffrey Morton. The modeling utilized for comparison was completed by Jeffrey Morton[17].

3.1.1 Quasi-Static Electromechanical

In order to quantify the stiffness characteristics of the system, transverse load versus transverse deflection curves were measured. The specimen was held in a custom fabricated, non-conductive 3-D printed mount. The specimen, shown in Figures 3.1a and 3.1b, was held in a manner to allow a deflection out-of-plane in a downward direction. The magnitude of the effective stiffness change was determined by measuring the transverse deflection simultaneously as the maximum loading on the inner ring of the specimen. During the tests, the voltage was applied to the specimen prior to loading and held constant throughout the subsequent loading repetitions. While the frequency of loading was vastly less than what would be observed in the iSprawl platform, this still allowed for a cyclic loading to monitor if any failure had occurred. The specimen was then deflected and allowed to return to the natural position. These experiments were performed at a constant deflection rate of 1.44 $\frac{mm}{s}$

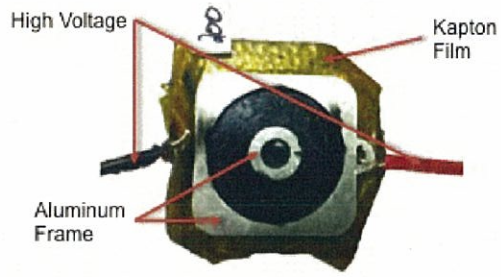

(a) A photograph of speciment used for testing. The leads from the amplifier are connected to the tabs of the upper frame and the lower frame (not visible).

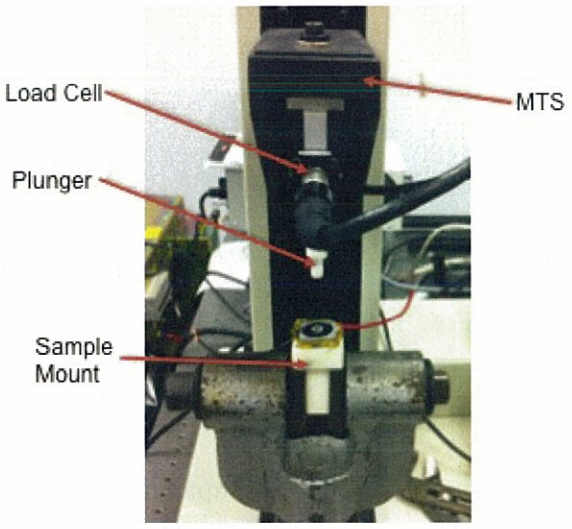

(b) Experimental setup of the MTS Insight machine. The machine is equipped with two custom made parts. The first being a 3-D printed mount to hold the specimen. The other being a delrin plunger to depress the inner ring of the module.

Figure 3.1: An individual module used for testing is shown in (a) and the testing apparatus is depicted in (b).

to a maximum deflection of 5 mm. The sampling rate of the data acquisition system was approximately 50 Hz. Once the load-deflection data was measured, the effective stiffness for each induced field was determined using a least square fit method in MATLAB^{TM}. The fit was performed from the starting point with an initial deflection of 0 mm and extended to the maximum load on the system. The voltages tested for all experiments ranged from the control (no voltage) and incrementally increased up till failure occurred. For membranes exhibiting higher degrees prestrains, the voltage increment was minimized during regions of potential failure. The response of the system due to the varying conditions was characterized by manipulating the applied voltages from 0 kV to a maximum of 9kV for the 200% prestrained sample. These voltages were obtained by amplification through a Trek model 10 kV/40 mA high voltage amplifier.

3.1.2 Transient Electromechanical

The transient testing was focused on investigating the response time of the system given a sudden field application or removal. The physical parameters of the system were practically identical to that seen in the quasi-static electromechanical experiments. The sample was held in place using the same non-conductive mount and tested using the MTS Insight. The difference arises during the voltage application. Rather than apply a constant field to the membrane then record the load-deflection data, the field was applied post-deflection. The sample plunger was moved through the downstroke to reach the maximum sample deflection of $5mm$ and was held stationary at this point for an extended time to prevent any load fluctuations during field application. The holding time was approximately 3 seconds. The field was then applied to the system, held for a period of time, and removed. During this process the data acquisition rate was approximately 500 Hz. This process was performed on a 400% prestrained sample with a field application of $5\frac{MV}{m}$.

3.2 Results and Discussion

3.2.1 Quasi-Static Electromechanical Results

The curves illustrated in Figure 3.2 show the 400% pre-stretched membrane as it is extended through the range of displacements measured on the MTS system. This is a representation of the raw data acquired prior to stiffness calculations. The upper line of each data set corresponds to the downstroke of the MTS pushrod and the lower line represents the upstroke or return to the zero load state. Over the downstroke section, a trendline was fitted to examine the linearity and illustrate field dependence on the stiffness change. With no applied field the data holds an R^2 correlation of 0.99. If the transverse load is related to the transverse stiffness using the relation $P = m(E)D$ where P is the load, D is the diplacement, and $m(E)$ is the slope as a function of the electric field, we measure a slope change of 92% between zero volts and a $6\frac{MV}{m}$ applied nominal field. When examining the sample exposed to a 7 $\frac{MV}{m}$ field, it can be seen the downstroke does not seem to begin until the plunger had already displaced approximately $3.5mm$. This is due to the occurrence of buckling. Upon field application the effective stiffness change was large enough that the elastic forces present in the membrane were not great enough to withstand the weight of the inner ring and unprovoked deflection occurred.

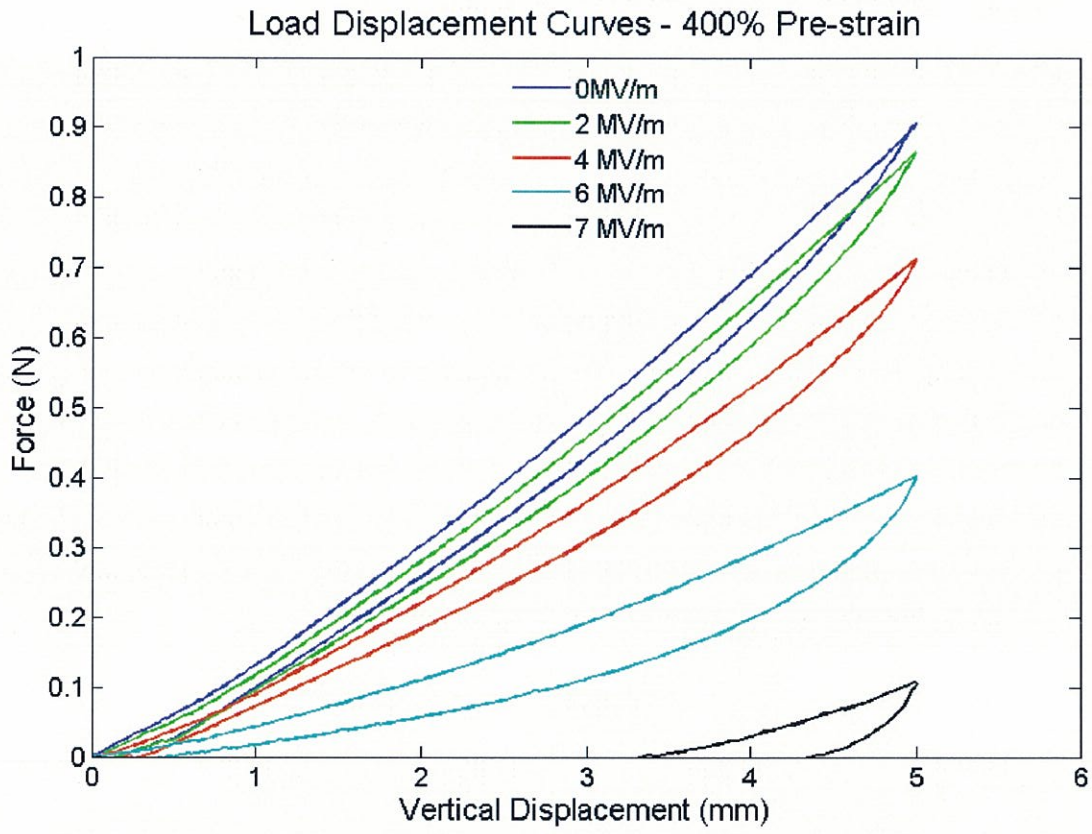

Figure 3.2: Load-Displacement curves for 400% pre-strained sample. It should be noted that over higher electric fields, the magnitude of the slope change increases with smaller field increments. The highest field application ($7\frac{MV}{m}$) only shows a force measurement after 3.5mm of deflection. This is due to buckling of the membrane.

To verify the results found, the experimental data was compared to expected stiffness values of the samples undergoing a zero field application. The expected values were obtained through the use of a Non-linear finite deformation membrane model. The correlation can be seen in Figure 3.3. In this Figure, the λ represents the stretch rate of the membrane. The stretch rate refers to the actual rate of deformation experienced by the membrane as compared to the rate of deflection experienced by the inner ring. The stretch rate varies radially along the prestretched membrane with the highest rate located at the boundary

of the inner ring. Because of this, an estimation was performed to approximate boundary encompassing the rate at which the membrane was actually being deformed. The upper and lower bounds, denoted by a λ of $9.4 * 10^{-1}s^{-1}$ and $5.64 * 10^{-1}s^{-1}$, respectively, act as the extreme values for the system. The experimental results can be associated with a stretch rate falling within this range. The figure clearly shows that the initial stiffness values of the various prestretches fit within the expected bounds predicted by the model.

The range of measured stiffnesses found from different field applications is illustrated in Table 3.1. Since each pre-stretch can affect dielectric breakdown, the voltage was incremented up to the field at failure. The reliability of higher prestrains is much lower than that of the less strained samples. In addition, smaller field increments tend to produce greater effects on the 400% sample as compared to the 300% and 200%. This results in a tendency for it to fail sooner and from smaller field increments. This led to the varying increments found in the 400% sample. The dashes in Table 3.1 represent values not tested for a particular reason. Prior experiments aided in providing information on the approximate failure points of the various prestrained membranes. For this reason, certain values were overlooked during testing because they did not represent a likely point of breakdown. For members demonstrating a higher degree of prestrain, the lowest stiffness value depicted represents the point after which failure occurs. For example, the final stable points for the 300% and 400% samples were approximately $0.06479\frac{N}{mm}$ and $0.01413\frac{N}{mm}$, respectively. Further testing is necessary to determine if higher fields are capable using smaller increments. From Table 3.1 and Figure 3.4, the overall change in effective stiffness can be calculated. The 200% specimen showed a maximum drop of approximately 30%. The percentage change increased with the amount of pre-stretch applied to the specimen, while the 300% and 400% pre-stretched modules exhibited approximate changes of 62% and 92% respectively. This suggests a linear relationship of 30% decrease in stiffness per 100% increase in prestretch.

The electro-mechanical tests were performed on each specimen while increasing voltage until dielectric breakdown occurred. With increasing pre-stretch the maximum achievable nominal field, applied voltage over original thickness (1 mm), decreases. The 200% specimen was capable of bearing the largest nominal field, failing at $9\frac{MV}{m}$. The 300% and 400% samples failed at $7.5\frac{MV}{m}$ and $7\frac{MV}{m}$, respectively. It is important to note, however, that due to decreasing membrane thickness with increasing pre-stretch, the true electric field over the 400% sample is nearly twice as large as the electric field over the 300% sample, and 4 times

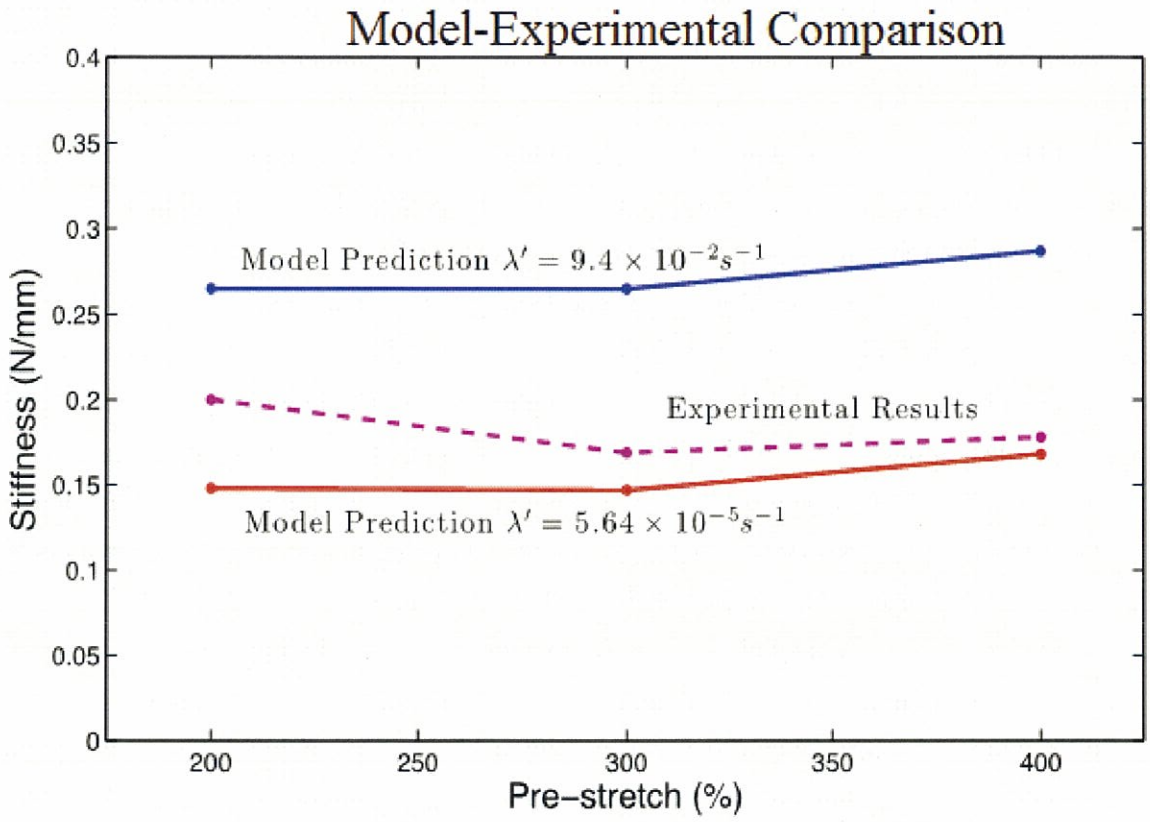

Figure 3.3: comparison of the model

the field over the 200% sample. The true fields can be estimated assuming incompressibility such that the actual thicknesses for the 200%, 300% and 400% pre stretches are $\frac{1}{4}, \frac{1}{9}$ and $\frac{1}{16} mm$ respectively. The resulting true fields are $36\frac{MV}{m}$, $72\frac{MV}{m}$ and $112\frac{MV}{m}$. These do not correspond exactly to the true field because the thickness changes as the field is applied.

3.2.2 Transient Electromechanical Results

In order to quantify the response time of the systems, the settling time was calculated from the load-displacement curve. It should be noted that the use of "settling time" infers the amount of time necessary to transition from the static load immediately prior to field application to within 1% of the final steady state value under electrostatic loading. The data acquired for 400% prestrain can be seen in Figure 3.5. The settling time was found to be in

Table 3.1: Plot representing the various stiffnesses experimentally determined based on amount of prestretch and field magnitude.

Field ($\frac{MV}{m}$)	200% Prestretch Stiffness (N/mm)	300% Prestretch Stiffness (N/mm)	400% Prestretch Stiffness (N/mm)
0	0.17882	0.16883	0.17044
1	-	-	0.16779
2	0.17848	0.16027	0.15942
3	0.17387	0.15355	0.14773
4	0.16830	0.14214	0.12962
5	0.16290	0.12582	0.10563
5.5	-	-	0.09087
6	0.15538	0.10677	0.06826
6.5	-	0.09573	0.04372
6.8	-	-	0.02066
7	0.14720	0.08216	0.01413
7.5	0.14180	0.06479	-
8	0.13594	-	-
8.5	0.13152	-	-
9	0.12604	-	-

the range of 66ms. Further characterization showed the module to have a natural frequency of approximately 55Hz. Notice should be taken to the amount of oscillation present within the system. Its behavior mimics that seen in an underdamped mass spring-damper system. Due to the vertical orientation of the sample, it is believed that the oscillatory motions could be caused by gravitational effects on the inner ring coupled with the drastically reduced compliance of the 400% sample. In order to counteract this, further testing should be performed in a horizontal orientation where gravity is no longer collinear with the direction of deflection. The relationship between system response and the field magnitude and amount of prestrain present could also be determined through more comprehensive testing.

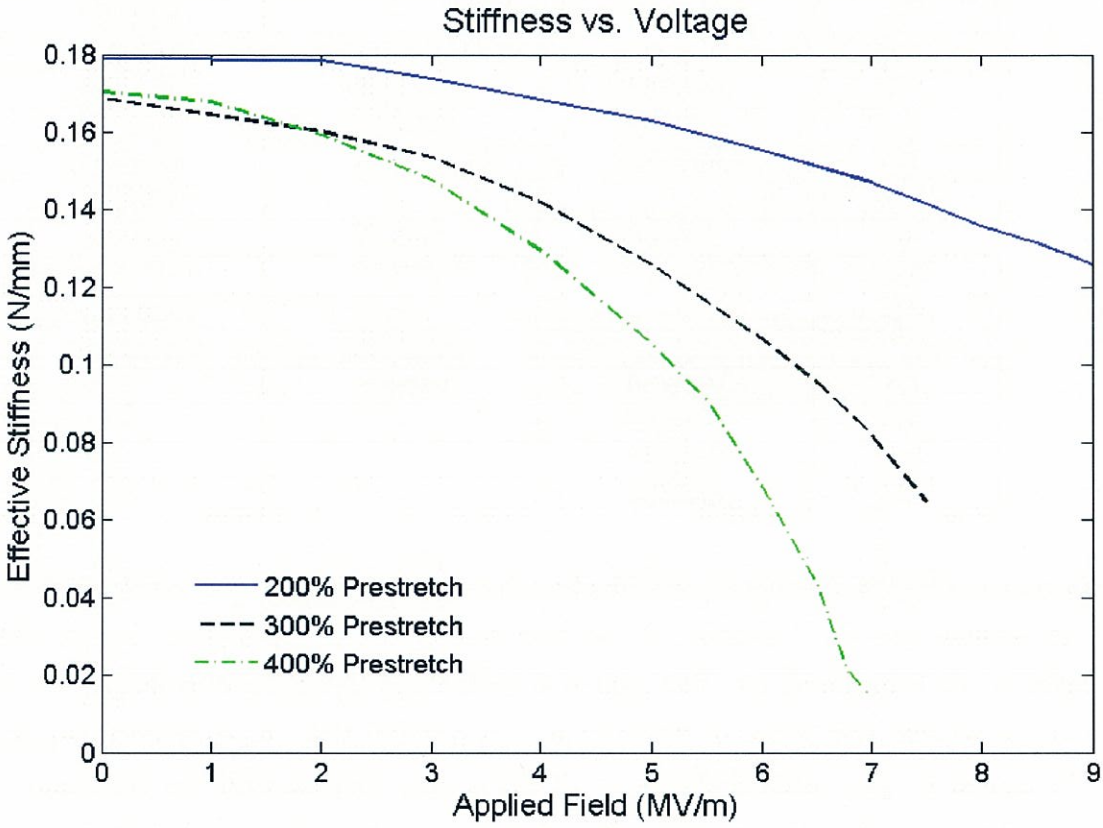

Figure 3.4: Average stiffness from various applied voltages

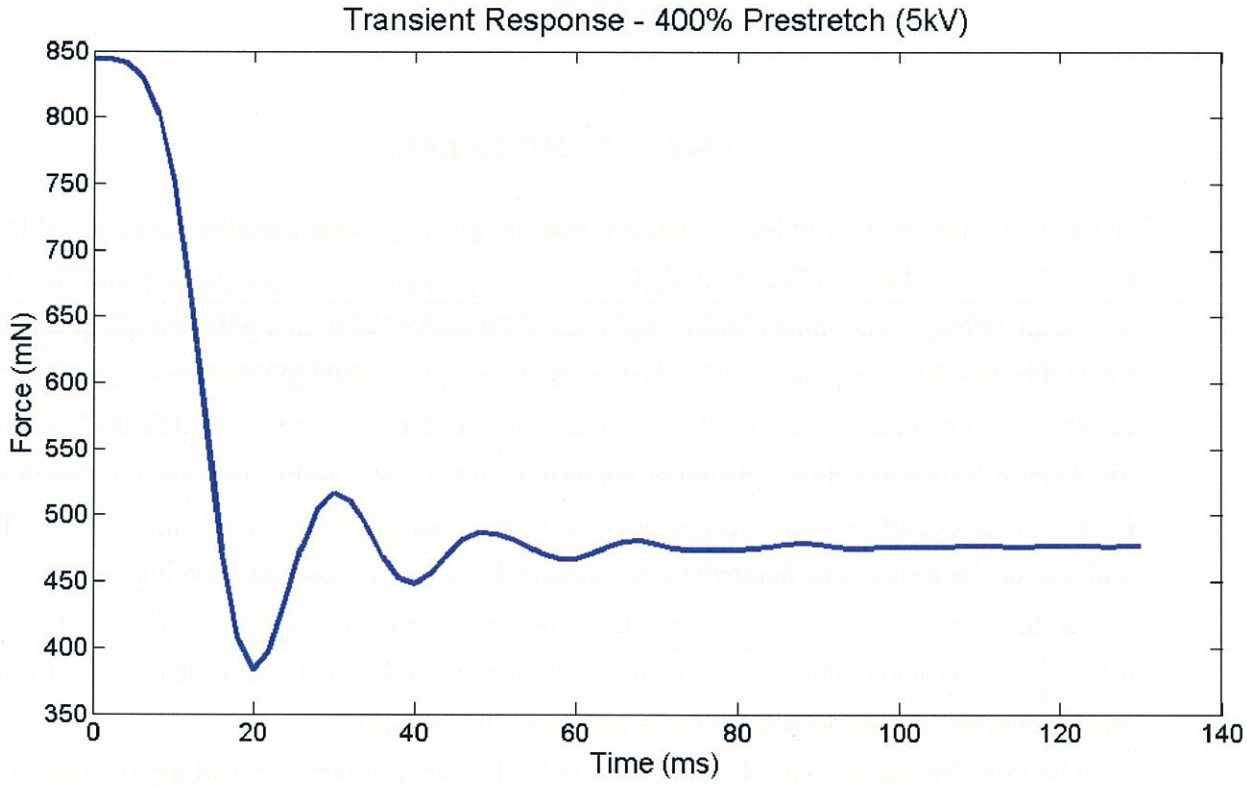

Figure 3.5: The transient response of a module prestrained to 400% and exposed to 5kV. The time required to transition from an unactuated state to the final load under a $5\frac{MV}{m}$ field is approximated at $66ms$.

CHAPTER 4

SUMMARY

4.1 Conclusion

A variable stiffness robotic leg mechanism was designed utilizing modules constructed from the dielectric elastomer VHB. It incorporated a diaphragm with suspended mounting rings to permit isolated attachment to the leg wires of iSprawl as well as modular implementation for highly tunable compliance. The system is the smallest VHB architecture developed for implementation onto a running robot. The design was characterized to identify its feasibility for robotic implementation. Stiffness changes of up to 92% were observed for individual models during electro-mechanical experiments using an applied voltage up to 9 kV. The stiffness of the design was dependent on prestretch, but it did not increase linearly. In fact, for modules prior to electric field exposure, it decreased from $0.20\ \frac{N}{mm}$ at 200% prestretch to $0.17\ \frac{N}{mm}$ at 300% and 400% pre-stretches. The electromechanical transient tests performed on the module showed an approximate response time of $66ms$.

The implementation onto iSprawl is bounded by two primary constraints; the deflection distance and the required stiffness range. The relative stiffness for iSprawl was set at $1.7\frac{N}{mm}$ and a desired leg stiffness variation of up to $1.1\frac{N}{mm}$ range was estimated from $0.85\frac{N}{mm}$ to $1.921\frac{N}{mm}$. With the results from the quasi-static electromechanical tests, the 400% sample demonstrated the greatest range and one of the highest initial stiffness values of approximately $0.17\frac{N}{mm}$. This suggests that approximately 6 modular elements pre-stretched to 400% could exhibit the required range of stiffness if connected in a parallel configuration. In order to achieve the minimum stiffness value, all 6 modules would be connected in parallel with a section of tubing approximating a spring constant of $0.85\frac{N}{mm}$. The deflection distance of 4 mm is encompassed by the test parameters established in this work, therefore series implementation should not be required for this application.

4.2 Future Work

In order to verify the designs viability for use in real world applications further testing is necessary. The design should be evaluated and optimized to enhance the stiffness characteristics with respect to the size and weight parameters. Furthermore, a more in depth investigation should be performed into the optimum stiffness for the iSprawl platform. Also, the design should be implemented in a parallel configuration and retested to investigate any unforeseen difficulties with multi-module integration. Cyclical loading tests are also needed to determine its lifespan and robustness. The transient results are questionable due to the possible dynamic influences of gravity on the inner ring of the system. Further quantification of the dynamic response due to field application is necessary to determine its frequency dependent limitations for the iSprawl platform. Upon determining the response time of the system, the designs capability to vary compliance mid stride will be analyzed. Upon completion of these tests, the design can be fully developed and tested on iSprawl to evaluate the level to which variable stiffness legs could improve its performance in running over various terrain types. The future form of the mechanism as it would be implemented onto iSprawl is shown in Figures 4.1a and 4.1b.

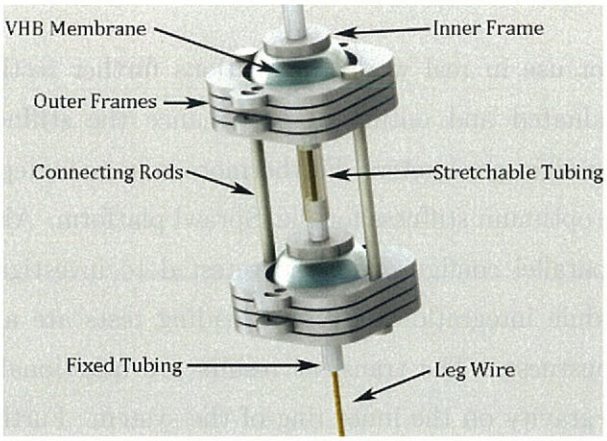

(a) Depiction of assembled iSprawl leg utilizing VHB modules

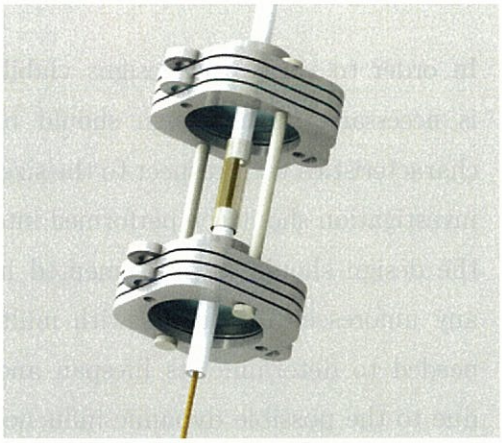

(b) Lower view of assembled leg design

Figure 4.1: iSprawl Leg design with variable stiffness assemblies. The modules shown are connected in a parallel orientation with a total of 6 membranes. 3 connected in parallel on the top and 3 on bottom. The leg wire routed through the center of the mechanism acts to deflect only the inner rings. Not shown here is the mounting system to isolate the outer frames.

Acknowledgments

This work been performed in part by Jeffrey Morton.

I would like to thank Jeffrey Morton, Dr. William Oates, Dr. Jonathan Clark, Michael Hays, Bruce Miller, James Dickson, and Michael Bunne for their roles in this project. I would also like to thank my thesis committee for their time and effort.

REFERENCES

[1] G. A. Cavagna, N. C. Heglund, and C. R. Taylor. Mechanical work in terrestrial locomotion: two basic mechanisms for minimizing energy expenditure. *American Journal of Physiology - Regulatory, Integrative and Comparative Physiology*, 233(5):R243–R261, 1977. 1.2.1

[2] R. McN Alexander. Three uses for springs in legged locomotion. *International Journal of Robotics Research*, 9(2):53–61, 1990. 1.2.1

[3] Daniel P. Ferris, Micky Louie, and Claire T.Ferris.1998 Farley. Running in the real world: adjusting leg stiffness for different surfaces. *Proceedings of the Royal Society of London. Series B: Biological Sciences*, 265(1400):989–994, 1998. 1.2.1

[4] Daniel P. Ferris and Claire T. Farley. Interaction of leg stiffness and surface stiffness during human hopping. *Journal of Applied Physiology*, 82(1):15–22, 1997. 1.2.1

[5] J.W. Hurst, J.E. Chestnutt, and A.A. Rizzi. The actuator with mechanically adjustable series compliance. *Robotics, IEEE Transactions on*, 26(4):597 –606, aug. 2010. 1.2.2, 1.2.2

[6] K. C. Galloway. *Passive variable compliance for dynamic legged robots.* PhD thesis, 2010. 1.2.2

[7] Mark Yim Kevin C. Galloway, Jonathan E. Clark and Daniel E. Koditschek. Experimental investigations into the role of passive variable compliant legs for dynamic robotic locomotion. *IEEE International Conference on Robotics and Automation*, 1243-1249, 2011. (document), 1.1, 1.2.2, 1.2, 2

[8] Qinghao Meng and Jinlian Hu. A review of shape memory polymer composites and blends. *Composites Part A: Applied Science and Manufacturing*, 40(11):1661 – 1672, 2009. (document), 1.2.3, 1.3

[9] Harper Meng and Jinlian Hu. A brief review of stimulus-active polymers responsive to thermal, light, magnetic, electric, and water/solvent stimuli. *JOURNAL OF INTELLIGENT MATERIAL SYSTEMS AND STRUCTURES*, 21(9):859–885, JUN 2010. 1.2.3

[10] Duncan Haldane. Design of a tunable stiffness leg for dynamic running using shape memory polymer. Master's thesis, 2011. (document), 1.2.3, 1.4

[11] J. Madden N. Vandesteeg, P. Anquetil, P. Madden, A. Takshi, R. Pytel, S. Lafontaine, P. Wieringa, and I. Hunter. Artificial muscle technology: Physical principles and Naval prospects. *IEEE J. Oceanic Eng.*, 29(3):706–728, 2004. (document), 1.2.3, 1.5

[12] Guggi Kofod. *Dielectric elastomer actuators.* PhD thesis, The Technical University of Denmark, 2001. 1.2.3

[13] Q Pei, M Rosenthal, S Stanford, H Prahlad, and R Pelrine. Multiple-degrees-of-freedom electroelastomer roll actuators. *SMART MATERIALS & STRUCTURES*, 13(5):N86–N92, OCT 2004. (document), 1.2.3, 1.2.3, 1.6

[14] Ron Pelrine, Roy Kornbluh, Qibing Pei, Scott Stanford, Seajin Oh, Joe Eckerle, Robert Full, Marcus Rosenthal, and Kenneth Meijer. Dielectric elastomer artificial muscle actuators: Toward biomimetic motion. *Proceedings of SPIE Smart Structures and Materials*, 4695:126–137, 2002. 1.2.3

[15] Sangbae Kim, Jonathan E. Clark, and Mark R. Cutkosky. isprawl: Design and tuning for high-speed autonomous open-loop running. *The International Journal of Robotics Research*, 25(9):903–912, 2006. 1.2.4, 2

[16] Sanjay Dastoor and Mark Cutkosky. Variable impedance due to electromechanical coupling in electroactive polymer actuators. In *Intelligent Robots and Systems (IROS), 2011 IEEE/RSJ International Conference on*, pages 774 –779, sept. 2011. 2.1

[17] Jason Newton, Jeffrey Morton, Jonathan Clark, and William S. Oates. Modeling and characterization of stiffness controlled robotic legs using dielectric elastomers. 2012. 3.1